Polarization in the 530.3 nm emission line and coronal magnetic field structure

O.G. Badalyan[1], V.N. Obridko[1] and J. Sýkora[2]

[1] *Institute of Terrestrial Magnetism, Ionosphere and Radio Wave Propagation, 142092 Troitsk, Moscow Region, Russia*

[2] *Astronomical Institute of the Slovak Academy of Sciences 059 60 Tatranská Lomnica, The Slovak Republic*

Received: January 15, 2002

Abstract. To clarify the possible influence of the coronal magnetic field on the degree of polarization p, direction of polarization β, and line intensity I_λ measured during the 11 July 1991 total solar eclipse, we have compared these quantities with different field parameters. The structure of the coronal magnetic field on the eclipse day was calculated using potential approximation. The relation of p and I_λ as measured at 1.2 $R_\odot$ from the centre of the solar disk to the strength of the magnetic field and its different components is discussed in detail. It is found that the points pertinent to the large-scale coronal structures of different morphological (physical) types (high-latitude streamers, bright equatorial regions, regions in the vicinity of coronal holes, etc.) form isolated, not overlapping clusters of points on the B – p, B – β and B – $\log I_\lambda$ diagrams. Two classes of objects are distinct in these diagrams. The first class comprises of high-latitude streamers in which the degree of polarization increases with decreasing B. The second class is represented by coronal condensations, moderately active equatorial regions, and coronal holes. In the objects of this class, the magnetic field strength is approximately three times as large as in the streamers, and the degree of polarization depends only weakly on B. It is shown that p, I_λ and β display a noticeable relationship with the indices Q_1 and Q_2, which we introduced to characterize the complexity (degree of inhomogeneity) of the magnetic field at any given point in the solar corona. In fact, Q_1 and Q_2 represent the absolute and relative deviations of B from its mean value measured in the neighbourhood of a given point.

The results of our investigation suggest that we are dealing with the direct influence of the magnetic field on the generation of the polarized radiation in the λ 530,3 nm emission line. One can expect, therefore, that the investigation of polarization characteristics would provide a useful method for determining the magnetic field in the solar corona.

Key words: coronal green line – polarization characteristics – coronal magnetic field

1. Introduction

The polarization measurements in the emission lines of the solar corona may substantially improve our understanding of the magnitude and structure of the coronal magnetic field. Measuring the emission line polarization is a rather complicated experimental problem, resulting in a relatively small amount of reliable observational data obtained. Therefore, new systematic spectral and filter space observations of the coronal polarization in different emission lines are highly desirable.

During the total solar eclipse on 11 July 1991 polarization filtergrams in the FeXIV λ 530.3 nm line were obtained and a polarization map for the whole corona was constructed (Badalyan and Sýkora, 1997a). A careful analysis of this map revealed some interesting peculiarities in the distributions of the coronal green line intensity and the degree and direction of its polarization. The original results are described in more detail in a number of papers (Badalyan and Sýkora, 1997a; Badalyan and Sýkora, 1997b; Badalyan *et al.*, 1997; Badalyan *et al.*, 1999a, 1999b, 1999c; Badalyan and Sýkora, 2001).

In two of our recent papers (Badalyan, 2002 – referred to here as Paper I, and Badalyan et al., 2002 – here as Paper II) we pointed out a serious discrepancy between the measured direction of polarization of the coronal green line radiation and that predicted by the currently accepted theory. In this paper (Paper III) we try to compare the line polarization p, intensity I_λ, and angle β with the strength and different components of the coronal magnetic field as calculated using potential approximation. It is demonstrated that the points corresponding to the bright coronal condensations, high-latitude streamers, and the regions in the neighbourhood of the coronal holes form separate clusters situated at distinctly defined positions on the diagrams representing the magnetic field B versus the degree of polarization p, B versus $\log I_\lambda$, and B versus β. On these diagrams, similarly to the $p - \log I_\lambda$ diagram in Badalyan et al. (1999a), two branches can be identified, one being, basically, related to the equatorial regions and another, to the high-latitude streamers. The conclusion about the clustered distribution of the points related to different types of the coronal features also remains true in the case of other magnetic field characteristics, particularly, in the case of the indices characterizing the magnetic field 'complexity' (degree of non-homogeneity) at a given distance from the limb in the regions where the large-scale coronal structures are situated. Thus, a pronounced relationship is observed between the coronal magnetic fields, on the one hand, and the characteristics of the green line polarization, on the other hand. This appaers to offer new possibilities for investigating the magnetic field in the solar corona.

Table 1. The list of the coronal structures under investigation.

No.	Structural feature	Position angle	Symbol in Figures
1	Coronal condensation	67–80	Open Circle
2	Coronal condensation	108–115	Star(*)
3	Coronal condensation	241–258	Cross(x)
4	Coronal condensation	272–287	Solid Circle
5	Equatorial region	84–107	Open Up Triangle
6	Equatorial region	119–129	Open Square
7	Equatorial region	259–268	Solid Square
8	NE–streamer	20–56	Open Down Triangle
9	SW–streamers	162–226	Solid Down Triangle
10	S coronal hole	133–138, 152–158	Solid Up Triangle
11	N coronal hole	313–317	Cross(+) inside Open Circle

2. Comparison of the coronal magnetic field strength with the green line polarization characteristics

Earlier (Badalyan et al., 1999a; Badalyan and Sýkora, 2001; Paper II), we studied the relationships between the polarization characteristics as measured in different types of the large-scale coronal objects, e.g., high-latitude streamers, bright coronal condensations, equatorial regions of moderate activity, and coronal holes.

Table 1 provides a list of 11 investigated coronal features together with their symbols used on the corresponding diagrams. It should be noted that we use the term "coronal hole" somewhat conditionally here, meaning, in fact, the close surroundings of the real coronal holes. This is because comparison of polarization with magnetic field is limited by the absence of the field data above $\pm 70°$ latitude. The coronal magnetic field was calculated using a well-known method described in earlier papers (Hoeksema and Scherrer, 1986; Hoeksema, 1993; see also Ivanov and Kharshiladze, 1994; Sýkora et al., 1999). We have software allowing us to compute all magnetic field components from the photospheric level up to the source surface at 2.5 $R_{\odot}$. Then, the synoptic charts of these components can be constructed for any date chosen as the centre of the chart. For the subsequent analysis, the magnetic field strength B and its different components, together with some complementary characteristics of the field, were computed for the eclipse day of 11 July 1991.

The basic results of our investigation of the relationship between the magnetic field strength B and its radial B_r and tangential B_t components, on the one hand, and the degree of polarization and the green line intensity, on the other hand, are presented in Figs. 1-3. The comparison described in this Section was done for the ring 0.03 $R_{\odot}$ wide situated at a distance of 1.2 $R_{\odot}$.

In Figs. 1a and 1b the diagrams of the field strength B versus the degree of polarization p and B versus the line intensity I_{λ} are plotted, respectively. The

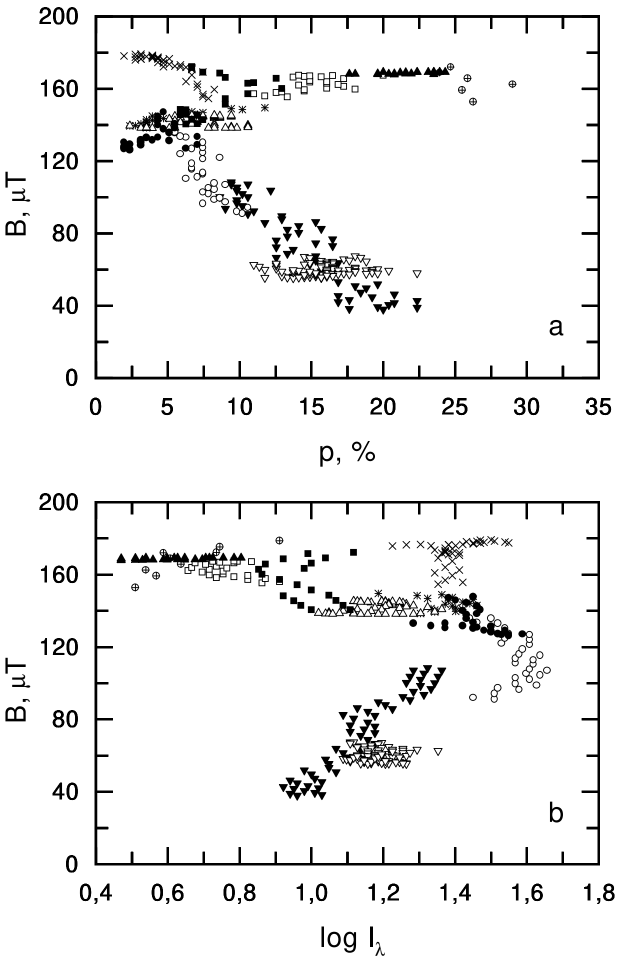

Figure 1. Comparison of the calculated coronal magnetic field strength B with the polarization p (a) and intensity $logI_\lambda$ (b) of the green line in different coronal objects (description of the objects and of the symbols used are in Table 1).

first conclusion that follows from Fig. 1 is that the points relevant to the particular coronal features form more or less compact clouds. This means that the extent of variations of the polarization characteristics under consideration and that of the magnetic field within each individual coronal feature is substantially smaller than it is for all the points inside the given narrow ring in the corona. This result completes and develops the idea of Badalyan et al. (1999a) that the two branches of the $p - \log I_\lambda$ anticorrelation diagram represent, in fact, a complex of separate clouds of points. Below, we shall demonstrate that such a peculiarity is typical of the comparison of the degree of polarization and line intensity with any other indices characterizing the coronal magnetic field.

In Fig. 1a, the following peculiarities in the distribution of points on the $B - p$ diagram can be noticed. When advancing from the small degrees of polarization to the larger ones, the points split into two branches at $p \approx 10\% - 12\%$. The bright coronal condensations, equatorial regions of enhanced activity, and regions surrounding the coronal hole are situated along the upper branch at the field strength $B > 120\ \mu T$. The polarization gradually increases when passing from the bright regions to the weaker ones and to the coronal holes. At the same time, the field strength B increases only slightly, being somewhat higher in the vicinity of coronal holes than in the equatorial structures.

In the field regions where $B < 100\ \mu T$, the high-latitude streamers of the 11 July 1991 corona are situated (see Fig. 1 in Paper II). It is evident that, in this branch, polarization distinctly increases with decreasing field strength. Within the north-east streamer (open down triangles), the field is practically constant, while the polarization varies from 12% to 25%. The points related to the system of the southern streamers (solid down triangles) form a prolonged band. The lowest cloud of points at $B < 40\ \mu T$ belongs to the near-pole streamer situated in the plane of the sky at $P \leq 208°$. At $60\ \mu T \leq B \leq 80\ \mu T$, the points belonging to the region of two overlapping streamers at $208° < P \leq 217°$ are situated. Then follows a transition to the second streamer, possibly situated outside the plane of the sky, at the northern basement of which a certain brightening on the X-ray image taken in the Fe XVI line during the SAO NIXT rocket experiment (Golub and Pasachoff, 1997) was observed. The points connecting both branches in the diagram (open circles – structure No. 1 in Table 1), belong to the bright coronal condensation at $60° < P < 80°$ at the east limb. On the white-light images, a short though bright equatorial streamer is visible there. This region, apparently, also represents transition from the high-latitude streamers to the coronal objects of the upper branch.

The negative correlation between the green line polarization and line intensity studied in Badalyan et al. (1999a) and Badalyan and Sýkora (2001) can be deduced by comparing Fig. 1a with Fig. 1b, the latter demonstrating diagram B–$\log I_\lambda$. Here again, one can readily see two branches joining in the region of the bright coronal condensation. Along the upper branch, the intensity varies by more than an order of magnitude with simultaneous small variations of the field. In the high-latitude streamers, the intensity variations are relatively small as compared to the field variations, which are about three times larger.

Thus, the analysis of Fig. 1 confirms the conclusion made by Badalyan et al. (1999a) that the two branches of the anticorrelation dependence between the degree of green-line polarization and intensity represent an aggregate of individual coronal features, where the clouds of points related to the different-type structures do not practically overlap. In this context, it is reasonable to assume that the two branches represent, in fact, the coronal objects of two basic classes. The first class comprises the objects in which the degree of polarization increases with decreasing B; the second class being represented by the objects in which the degree of polarization depends only weakly on B. Within each class, every object creates a separate cluster of points. The nature of the two branches is discussed below.

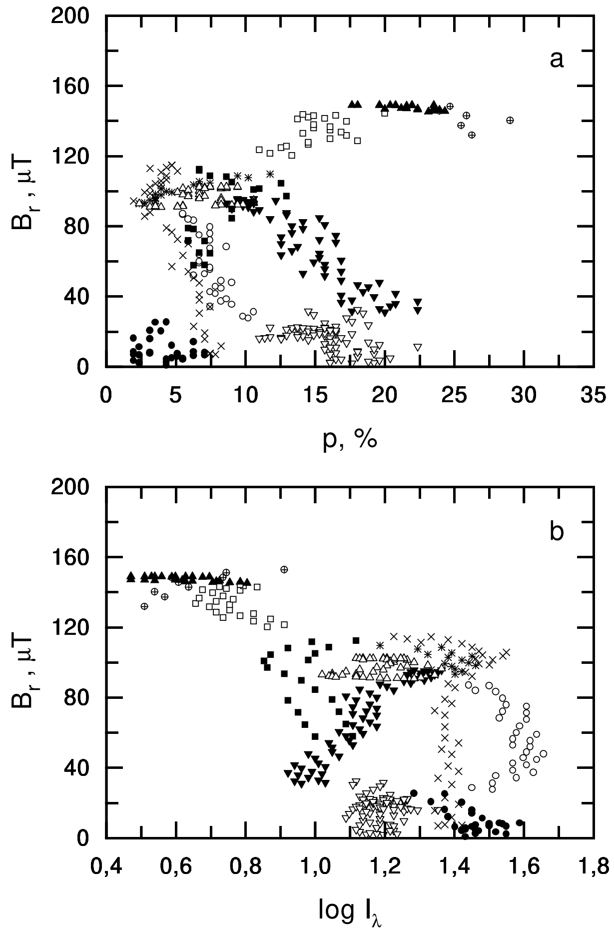

Figure 2. The same as in Fig. 1 for the radial component of the field B_r. The signs of this component are neglected.

The similar diagrams, constructed for the radial B_r and tangential B_t components of the field are presented in Figs. 2 and 3. The sign of the radial component B_r is neglected. Here, the clustered distribution of the points relevant to different coronal features is also well pronounced, particularly, in Fig. 3. Within the structures of the first class, the radial field B_r increases when passing from the bright features to the coronal holes (Fig. 2). In this case, the polarization is almost constant at $p < 10\%$ up to the values of the radial component $B_r \sim 100\ \mu T$. Then, polarization increases rapidly with the increasing field strength. The splitting is less pronounced in the diagram for the radial component than in the diagram for the field strength B in Fig. 1.

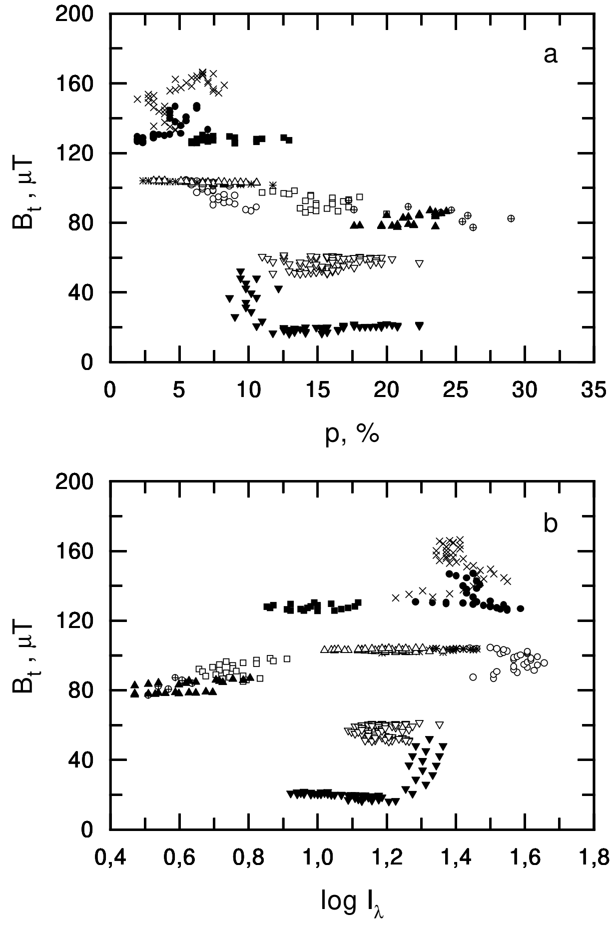

Figure 3. The same as in Fig. 1 for the tangential component of the field B_t.

The tangential component B_t (Fig. 3) does not, actually, change within each of the coronal objects, with the exception of the points belonging to the system of the southern streamers at $217° < P \leq 226°$, where brightening in the Fe XVI line was observed (see above). In the high-latitude streamers, the tangential component as well as the magnetic field strength are smaller in comparison with the second class objects. These second class objects exhibit the highest B_t values and the lowest values of polarization p within the bright objects, while the highest polarizations p and small B_t values are found in the vicinity of the coronal holes. A weak increase of the total field strength B in these objects is caused by an increase of the radial component.

The nature of the two branches is, apparently, controlled by the magnetic field and depends on the actual ratio of closed (loop-like) and open structures. We believe that the degree of 'complexity' (a degree of the non-homogeneity) of the magnetic field in the structural elements of the corona is crucial for explaining the observed effects. If the magnetic field inside a given object can be considered quasi-homogeneous, not strongly variable in direction and strength, a high linear polarization can be expected. Such a case is realistic in the huge high-latitude streamers and coronal holes. The bright coronal condensations consisting of a number of relatively low loops are another extreme case. Here, the magnetic field is remarkably non-homogeneous and a low polarization should be expected.

To verify these ideas, we have compared our Fig. 1 representing the B–p and B–$\log I_\lambda$ relations with the synoptic charts constructed from the magnetic field data of the Wilcox Solar Observatory (Stanford) for the photospheric and the source surface levels, and the Mount Wilson and Kitt Peak magnetograms obtained on July 4 and 18, 1991 (these dates correspond to the west and east limb passages of the eclipse day central meridian), taken from SGD. The comparison revealed that the splitting into two branches seen in our figures, as well as the presence of two branches in the p–$\log I_\lambda$ diagram (Badalyan et al. 1999a), are mutually related and are, indeed, determined by the contribution of the closed and open configurations and the magnetic field strength. Moving up along the lower branch of the B–p diagram (Fig. 1a) from right to left, we advance from the streamers, where the magnetic field structure is relatively simple and is mostly represented by high loops, to the active regions, where the role of the closed fields is larger and, at the same time, the field strength increases substantially. On the B–$\log I_\lambda$ diagram (Fig. 1b), the intensity increases remarkably when passing from the streamers to the active regions. Therefore, on the p–$\log I_\lambda$ diagram in Badalyan et al. (1999a), this corresponds to the decrease of polarization with increasing intensity. The growth of the degree of polarization along the lower branch is possibly connected with the increased contribution of the polarized component of radiation in the less dense structures.

The upper branch starts in the active regions and is determined by the gradually decreasing role of the closed fields with a simultaneously constant fairly high field strength. This branch corresponds to the transition from the active regions, through the regions of dispersed local fields of relatively large strength, to the regions around the coronal holes. The magnetic field along this branch remains permanently high, though its structure changes from strongly variable near the active regions to the relatively well-arranged in the vicinity of the coronal holes. On the B–p and B–$\log I_\lambda$ diagrams, this transition corresponds to a considerable increase of polarization (i.e., a considerable decrease of brightness) with a moderate increase of the magnetic field. This branch corresponds to the lower branch of the anticorrelation dependence between the polarization and the green-line intensity on the p–$\log I_\lambda$ diagram.

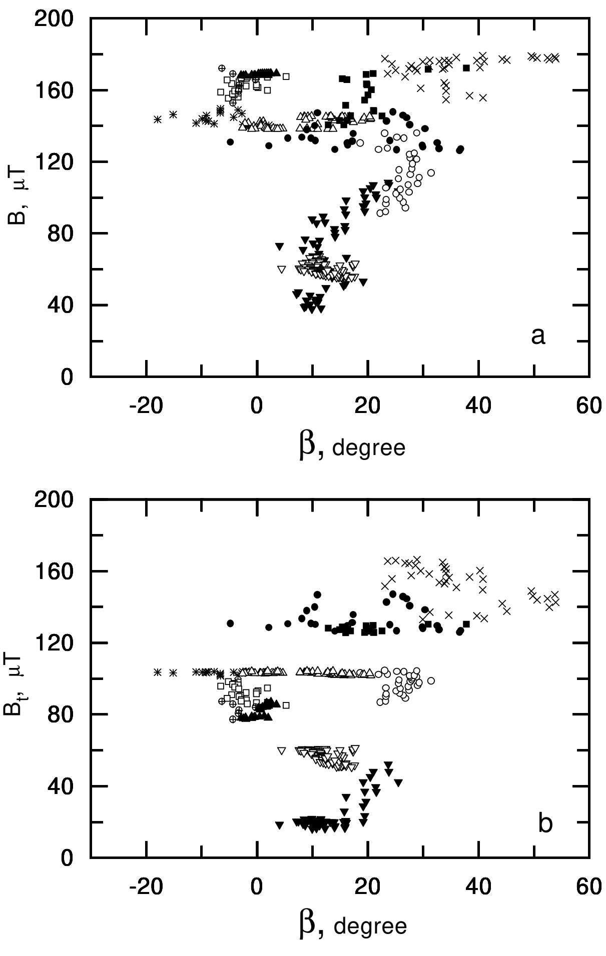

Figure 4. Comparison of the deviation angle of the plane of polarization β (magnetic vector) with the calculated coronal magnetic field strength (a) and the tangential component of the field (b).

Let us also compare the angle β with some coronal magnetic field characteristics. In Fig. 4, β is compared with the magnetic field strength B and with the tangential component B_t. Fig. 4a shows that the dispersion of β increases with growing field strength, and the angle itself reaches fairly large magnitudes.

The high-latitude streamers are located in the region of small fields and small β values. In the vicinity of the coronal holes and inside the bright equatorial objects, the field is about equally high, however, it affects the deviation of the plane of polarization (magnetic vector) from the radial direction in a different way. Part of the southern streamers (solid down triangles) at $217° \leq P \leq 226°$ with an active region at the base and the east-limb coronal condensation at $67° \leq P \leq 80°$ with a bright short streamer above it are transient structures between the streamers and the active equatorial regions.

Comparison of the β angles with the tangential component of the magnetic field B_t (Fig. 4b) shows that this component substantially influences the deviation of the plane of polarization from the radial direction, in contrast with the radial component B_r (we do not present this comparison here, owing to the small amount of information contained). As in Fig. 3b, it is evident that the tangential component of the field changes very little within each of the coronal objects. The only exception is the part of the south-west streamer with activity at its base. The B_t component is small in the streamers and is largest in the equatorial objects at the west limb. The clustered distribution of the points related to different coronal structures is, as earlier, seen in these figures.

3. Other magnetic field indices

The comparison of the polarization p, green line intensity I_λ, and angle β with the magnetic field strength B and with the different field components described above revealed a definite relationship of these quantities with the magnitude of B and, apparently, with a certain characteristic of the field we arbitrarily designated as 'the field complexity' (i.e., the degree of the field inhomogeneity). To check the relationship of p and I_λ with this parameter, we have introduced additional indices characterizing the complexity of the field. They can be calculated if all the magnetic field components are known.

The analysis of the magnetic field synoptic chart calculated for the height of $1.2\ R_\odot$ has shown that the isolines of the B values are much more rarefied in the regions where the high-latitude streamers are situated than in those occupied by the equatorial coronal condensations. This means (as was to be expected) that the field inside the streamers changes with position angle more slowly than it does in the equatorial regions. Therefore, the first index we have introduced represents a measure of the field variability over a certain part of the solar surface. The B values on the synoptic chart were averaged over an area $9° \times 9°$ for each point on the limb, points being spaced $1.4°$ apart, i.e. the moving average $\bar{B}$ was determined. Then, the mean square deviation was calculated for the same points and was adopted as the Q_1 index:

$$Q_1 = \sqrt{\frac{(B_i - \bar{B})^2}{n-1}}, \tag{1}$$

where B_i is the field strength at the i-point and n is the number of points over the area $9° \times 9°$.

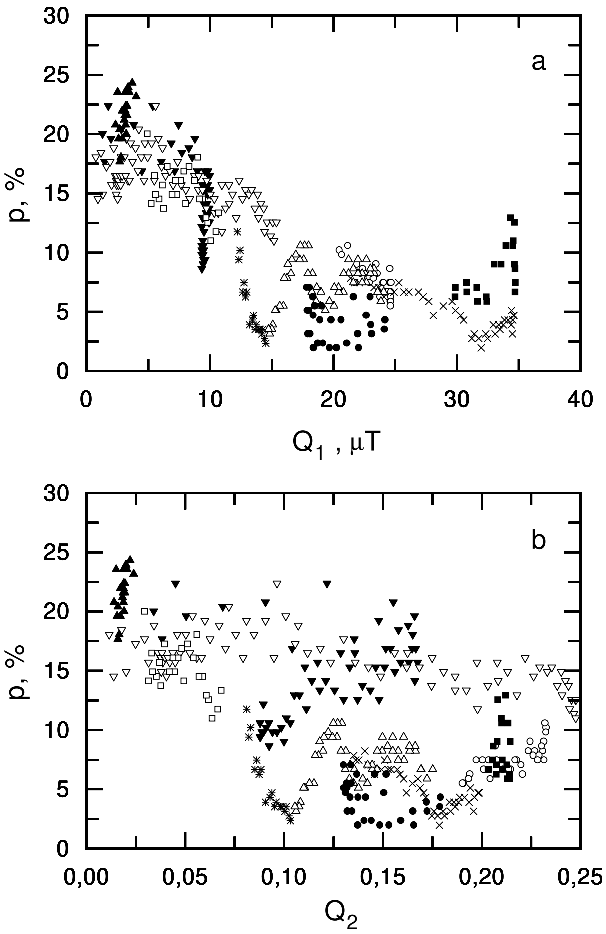

Figure 5. The degree of polarization versus the indices of complexity (degree of inhomogeneity) of the magnetic field: absolute (a) and relative (b) mean square deviations of the magnetic field strength from its mean value in the vicinity of a given point.

In Fig. 5a, the polarization p is compared with the Q_1 index for all the coronal objects identified. The figure reveals a pronounced relationship between the field 'complexity' of any chosen coronal object and the degree of polarization within it: the higher the field variability around a given point in the corona (which we interpret as the field 'complexity') the lower the degree of the green line polarization at that point. Note, however, that the points in the vicinity of the northern coronal hole do not obey this general law and are not presented in Fig. 5a. The clustered pattern persists in the diagram in Fig. 5a, however, the dependence of p on Q_1 is one-dimensional, i.e., there is no splitting into two branches.

As the Q_2 index, we have used the relative mean square deviation:

$$Q_2 = \frac{1}{\bar{B}}\sqrt{\frac{(B_i - \bar{B})^2}{n-1}}. \quad (2)$$

The comparison of the polarization p and the Q_2 index is shown in Fig. 5b. Here, the relationship again splits into two branches. The upper branch contains the high-latitude streamers and the lower one, the near-equatorial objects and the points in the vicinity of the southern coronal hole. The NE–streamer (white point down triangles) covers the whole range of variability of the Q_2 index. The SW–streamers (solid down triangles) at $200° \leq P \leq 217°$ are partly situated along the upper branch within $0.10 < Q_2 < 0.17$, while the transition to the lower branch takes place at $217° < P \leq 226°$ where a brightening is observed on the image taken in the line Fe XVI.

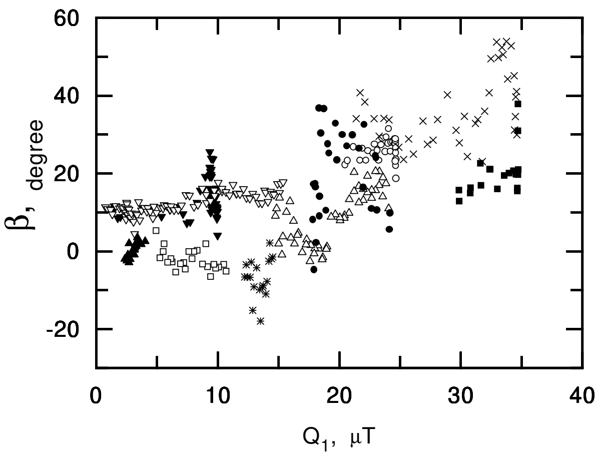

Figure 6. Comparison of the deviation angle of the plane of polarization with the index characterizing a degree of the field inhomogeneity, i.e., with the absolute mean square deviation of the field strength from its magnitude in the vicinity of a given point.

Figure 6 illustrates β versus Q_1. One can clearly see that the increase of field complexity is accompanied by an increase of the angle β, which becomes exclusively positive beginning with $Q_1 \geq 20\ \mu T$. The comparison of β with the Q_2 index has a similar character.

Table 2. The mean polarization and magnetic field parameters (expressed in μT) in the different coronal structures. Understandably, Q_2 is dimensionless.

No.	Structural feature	p, %	$\log I_\lambda$	β	B	B_r	B_t	Q_1	Q_2
1	Coronal condensation	7.6	1.57	26.0	113	57	97	23.5	0.22
2	Coronal condensation	5.4	1.37	-6.9	144	100	103	13.4	0.09
3	Coronal condensation	5.1	1.40	36.6	172	71	152	29.6	0.17
4	Coronal condensation	4.1	1.46	19.7	134	10	134	20.2	0.15
5	Equatorial region	7.3	1.18	8.7	142	97	103	19.6	0.14
6	Equatorial region	15.1	0.76	-2.2	162	134	92	7.8	0.05
7	Equatorial region	8.3	0.98	19.9	156	88	128	33.1	0.21
8	NE–streamer	15.9	1.19	12.3	60	16	57	7.3	0.02-0.25
9	SW–streamers:								
	$200 \leq P \leq 208$	19.2	0.99	11.4	44	39	21	5.5	0.12
	$208 < P \leq 217$	14.6	1.13	11.7	71	68	19	9.8	0.14
	$217 < P \leq 226$	10.4	1.29	18.3	99	92	35	9.4	0.09
10	S coronal hole	21.7	0.61	0.5	169	148	82	3.1	0.02
11	N coronal hole	25.9	0.58	-3.6	164	141	83	25.8	0.16

As follows from Figs. 5 and 6, the degree of the field inhomogeneity is an important parameter affecting both the degree and direction of the green line polarization. The mechanism of this relationship is not very clear. It could be due to the influence of the magnetic field both on the formation of large-scale coronal structures and on the origin of the line polarization (including a possible effect of the electric currents). At the same time, a combined contribution of the coronal structures of different size to global radiation should be considered owing to integration along the line of sight.

The mean green-line polarization parameters, such as the degree of polarization p, intensity I_λ, and angle β, together with the parameters and complementary indices of the coronal magnetic field as derived for the large-scale coronal structures under consideration, are listed in Table 2.

4. Conclusions

To investigate the possible effect of the magnetic field on the origin of polarization in λ 530.3 nm radiation, the measured degree of polarization p, line intensity I_λ, and direction of the plane of polarization (angle β) were compared with the calculated magnetic field strength B and with some other field indices. The comparison was carried out for 11 large-scale structures of different level of activity identified in the 11 July 1991 corona. All the points analyzed were situated inside a narrow ring at a fixed distance from the solar disk centre. The structure of the coronal magnetic field was calculated under potential approximation for the eclipse day and for the distance 1.2 $R\odot$.

The comparison of p, I_λ, and β with the magnetic field strength B revealed that the points related to the large-scale structures of different types are distributed on the $B - p$ and $B - \log I_\lambda$ diagrams in the form of individual, non-overlapping clouds (clusters) of points. Such a clustered character of the distributions of points is also typical of different magnetic field components and of the complementary indices we introduced. Two classes of coronal objects can be identified in the diagrams. The first class of objects are represented by the high-latitude streamers, which form the upper branch in the $p - \log I_\lambda$ diagram in Badalyan et al. (1999a). In these objects, polarization increases when magnetic field strength decreases. The radial component of the field B_r considerably increases within this first class of objects when advancing from the bright structures to the coronal holes. The longitudinal component B_t is almost constant within each of the objects.

The second class of objects is represented by the bright coronal condensations, equatorial regions of moderate activity, and coronal holes. Within these objects, the degree of polarization only slightly depends on the field strength B which, in this case, is about three times higher than that in the streamers.

To clarify the observed regularities, we have introduced the Q_1 and Q_2 indices characterizing 'the complexity' (the degree of inhomogeneity) of the magnetic fields in the structural coronal elements under consideration – respectively, the absolute and relative mean square deviations of B from its value, averaged over a certain area surrounding a given point. A close mutual relationship of p and β with the Q_1 index was found. If the index of the field inhomogeneity Q_1 increases, the degree of polarization decreases and the β angle increases, both creating more or less linear dependence. A similar tendency though not as clear, exists on the $p - Q_2$ diagram. At the same time, another characteristic peculiarity arises – the two branches appear, reminding the two branches found in Badalyan et al. (1999a) and corresponding to the two classes of objects considered in this article.

This analysis shows that a physical connection probably exists between the parameters determining the strength and structure of the magnetic field and the characteristics of the green line polarization. This means that the polarization characteristics we have derived reflect in a certain way the real parameters of the coronal magnetic field. Therefore, we can give approximate magnitudes of the magnetic field strength for the two most typical objects in the corona: 50 μT for the high-latitude streamers and about three times more for the bright coronal condensations, both estimated for the height 1.2 $R_\odot$.

The relationship between the polarization and the magnetic field was, in principle, theoretically predicted in the papers by Rachkovsky (1967), House (1974), and House et al. (1982) and in the monograph by Stenflo (1994). However, the verification of such a relationship was difficult due to the absence of direct measurements of the magnetic field in the corona. This study actually confirms the existence of the relationship. In addition, the investigation and full understanding of coronal line polarization may possibly become a method of measuring the coronal magnetic field. Of course, the correlations found in our study are based on very simplified calculations of the magnetic field strength. Nevertheless, the described picture seems to be quite real, and the scheme of the magnetic field influence on the line scattering (the influence of the magnetic field complexity on the magnitude of polarization) becomes qualitatively understandable. Despite this optimistic view, there still remains the serious problem of the discrepancy between the theory of polarization and the observational results (Badalyan et al., 2002; Paper I).

Acknowledgements. This work was supported by the grants No. 99-02-18346 of the Russian Foundation for Basic Research, and the VEGA grant 2/1022/21 of the Slovak Academy of Sciences.

References

Badalyan, O.G.: 2002, *Contrib. Astron. Obs. Skalnaté Pleso* **32**, 39 - Paper I

Badalyan, O.G., Sýkora, J.: 1997a, *Astron. Astrophys.* **319**, 664

Badalyan, O.G., Sýkora, J.: 1997b, in *Theoretical and Observational Problems Related to Solar Eclipses, NATO ASI Series C: Mathematical and Physical Sciences* **494**, eds.: Z. Mouradian and M. Stavinschi, Kluwer Academic Publishers, Dordrecht, 25

Badalyan, O.G., Sýkora, J.: 2001, *Pisma Astron. Zh.* **27**, 521 (*Astron. Letters* **27**, 445)

Badalyan, O.G., Beigman, I.L., Livshits, M.A.: 2001, *Astron. Zh.* **78**, 373 (*Astron. Reports* **45**, 321)

Badalyan, O.G., Livshits, M.A., Sýkora, J.: 1997, *Astron. Zh.* **74**, 767 (*Astron. Reports* **41**, 682)

Badalyan, O.G., Livshits, M.A., Sýkora, J.: 1999a, *Astron. Astrophys.* **349**, 295

Badalyan, O.G., Obridko, V.N., Sýkora, J.: 1999b, *Astron. Zh.* **76**, 869 (*Astron. Reports* **43**, 767)

Badalyan, O.G., Obridko, V.N., Sýkora, J.: 1999c, in *Solar Polarization, Proc. SPW2*, eds.: K.N.Nagendra and J.O.Stenflo, Kluwer Academic Publishers, Dordrecht, 373

Badalyan, O.G., Obridko, V.N., Sýkora, J.: 2002, *Contrib. Astron. Obs. Skalnaté Pleso* **32**, 49 - Paper II

Golub L. , Pasachoff J.M.: 1997, *The Solar Corona (cover illustration)*, Cambridge Univ. Press, Cambridge

Hoeksema, J.T.: 1993, in *Solar Terrestrial Predictions - IV*, ed.: J. Hruska, M.A. Shea, D.F. Smart, G. Heckman, NOAA/ERL, Boulder, 3

Hoeksema, J.T., Scherrer, P.H.: 1986, *The Solar Magnetic Field – 1976 through 1985*, WDCA Report UAG-94, NGDC, Boulder

House, L.L.: 1974, *Publ. Astron. Soc. Pac.* **86**, 490

House, L.L., Querfeld, Ch.W., Rees, D.E.: 1982, *Astrophys. J.* **255**, 753

Ivanov, K.G., Kharshiladze, A.P.: 1994, *Geomagnetizm and Aeronomia* **34**, 22

Rachkovsky D.N.: 1967, *Izv. Krymskoj Astrofiz. Obs.* **36**, 3

Stenflo J.O.: 1994, *Solar Magnetic Fields. Polarized Radiation Diagnostics*, Kluwer, Dordrecht

Sýkora, J., Badalyan, O.G., Obridko, V.N., Pintér, P.: 1999, *Contrib. Astron. Obs. Skalnaté Pleso* **29**, 89